

# From Bloch Oscillations to a Steady-State Current in Strongly Biased Mesoscopic Devices

J. M. Alendouro Pinho,<sup>1,2,\*</sup> J. P. Santos Pires,<sup>1,2</sup> S. M. João,<sup>1,2,3</sup> B. Amorim,<sup>4</sup> and J. M. Viana Parente Lopes<sup>1,2,†</sup>

<sup>1</sup>*Departamento de Física e Astronomia, Faculdade de Ciências da Universidade do Porto, Rua do Campo Alegre, s/n, 4169-007 Porto, Portugal*

<sup>2</sup>*Centro de Física das Universidades do Minho e do Porto (CF-UM-UP) and Laboratory of Physics for Materials and Emergent Technologies LaPMET, University of Porto, 4169-007 Porto, Portugal*

<sup>3</sup>*Department of Materials, Imperial College London, South Kensington Campus, London SW7 2AZ, United Kingdom.*

<sup>4</sup>*Centro de Física das Universidades do Minho e do Porto (CF-UM-UP) and Laboratory of Physics for Materials and Emergent Technologies LaPMET, Universidade do Minho, 4710-057 Braga, Portugal*

It has long been known that quantum particles moving in a periodic lattice and subject to a constant force field undergo an oscillatory motion that is referred to as Bloch Oscillations (BOs). However, it is also known that, under quite general conditions, a biased mesoscopic system connected to leads should settle in a steady-state regime characterized by a constant electric current (described by the Landauer formula). Since both effects are driven by a constant field, these two quantum transport phenomena appear to be at odds with each other. Here, we solve this apparent contradiction by theoretically demonstrating that BOs can actually be observed in biased two-terminal mesoscopic devices as a transient phenomenon, which relaxes for long times to a steady-state current that agrees with the Landauer formula. Furthermore, we also combine analytical and numerical time-evolution results for a one-dimensional tight-binding model of a biased two-terminal mesoscopic system, in order to characterize the decay times of the transient BOs and establish the conditions under which they can occur.

## I. INTRODUCTION

When electrons moving in a periodic lattice are accelerated by a constant electric field, they give rise to oscillatory currents. This long-established phenomenon is referred to as *Bloch oscillations*<sup>1;2</sup> (BOs) and is expected for any quantum particle that moves across a periodic background potential in the presence of an uniform driving force (see Glück *et al.*<sup>3</sup> for an extensive review). Despite being theoretically well understood, the experimental observation of BOs remains an outstanding challenge in solid-state systems<sup>4</sup>. The fragility of electronic BOs in solid-state systems results from the fact that their period (inversely proportional to the applied field) is typically much larger than the electronic scattering times, thus leading to a loss of phase-coherence before a single current oscillation can be finalized. As such, to this day electronic BOs have only ever been detected in synthetic semiconducting superlattices<sup>5–8</sup>. Analogues of BOs have been observed in a variety of alternative platforms, such as modulated photonic waveguides<sup>9–14</sup>, arrays of coupled acoustic cavities<sup>15;16</sup>, ultra-cold atoms in optical potentials<sup>17–19</sup>, and even in superconducting *q-bit* arrays<sup>20</sup>.

On the other hand, it is also expected that in a mesoscopic system connected to electrodes at different electrochemical potentials, an electric current will begin to flow, which eventually reaches a steady-state regime.

As first argued by Landauer<sup>21;22</sup>, and later generalized by Büttiker<sup>23</sup>, the steady-state current flowing between the electrodes is proportional to the quantum transmittance of the sample: a *non-local* property that is sample-specific and strongly depends on the precise geometry of the device<sup>24;25</sup>. This result is the celebrated *Landauer formula*, which was later demonstrated<sup>26;27</sup> to yield the same steady-state current as the one derived by Caroli *et al.*<sup>28</sup>, using a non-equilibrium Green's function formalism. It is important to note that both these approaches assume that the system reaches a non-equilibrium steady-state, making no attempts to describe how (or whether) this state is reached. It was later theoretically demonstrated that a non-equilibrium steady-state is reached provided the electrodes have a smooth non-zero density of states<sup>29</sup> and that there are no bound states in the mesoscopic device<sup>30;31</sup>. A smooth density of states in the leads gives origin to a loss of memory of the initial state of the system. Bound states, in turn, give origin to oscillating behavior in the current. The establishment of a steady-state in biased mesoscopic system, after an initial transient regime, has been theoretically demonstrated in systems with and without inelastic mechanisms, assuming that the current is driven by either the lead-sample couplings (*partitioned setup*)<sup>32</sup> or a static electric field that is suddenly applied across the device (*partition-free setup*)<sup>29;33;34</sup>.

The dynamics of current in the transient regime that precedes the steady-state have been subject of increasing interest<sup>31;35–47</sup>. The transient regime has been shown to unveil exotic quantum effects that are otherwise washed out in the steady-state. Two remarkable exam-

\* up201703751@fc.up.pt

† jlopes@fc.up.pt

ples of this are: (i) the ability to distinguish the signatures of Andreev and quasi-Majorana states in quantum transport data of superconducting nano-wires<sup>41</sup>, and (ii) the description of time-dependent radiation from biased nano-antennas<sup>45</sup>. These studies were made possible by the recent development of numerical time-dependent Landauer-Büttiker methods<sup>36;40;44;48–50</sup>.

Since the current dynamics of a biased mesoscopic system naturally relax towards a steady-state current, the question of whether BOs can be seen in these devices naturally arises. In a prior work, Popescu and Croy<sup>51</sup> have theoretically shown that persistent Bloch oscillations *can occur* in mesoscopic devices at very strong electric fields. However, in this proposal, BOs only exist when the applied electric field is such that there is a total reflection of electrons with no net current flowing through the device. Hence, one might ask if this is always the case or whether a mesoscopic device can also exhibit Bloch oscillations as a *transient regime* which eventually relaxes to a steady-state, described by the Landauer formula. The goal of this work is to determine the conditions in which such *transient Bloch oscillations* (tBOs) are possible in a mesoscopic device. In order to do so, we study a one dimensional tight-binding chain, combining numerical quantum time-evolution<sup>40;44;52</sup> with quantum transmittance calculations<sup>53</sup>. The results are then physically interpreted on the basis of (i) Wannier-Stark localization induced by strong electric fields within the mesoscopic sample, and (ii) scattering states and wavefunction matching.

The remaining of this paper is structured as follows: In Sec. II, we outline the model Hamiltonian considered and the numerical method used for quantum time-evolution. The main numerical results showing the tBO regime are presented in Sec. III. The decay times of the tBOs are computed within a quasiparticle approximation in Sec. IV. Finally, in Sec. V we summarize our key findings.

## II. MODEL AND METHODS

### A. Hamiltonian and initial state of the Mesoscopic Device

We will consider transport through a one dimensional mesoscopic system, which we described by a tight-binding model given by

$$\mathcal{H}(t) = \mathcal{H}_C(t) + \sum_{\alpha=L,R} \mathcal{H}_\alpha(t), \quad (1)$$

where  $\mathcal{H}_C$  describes the central sample,  $\mathcal{H}_{L(R)}$  is the Hamiltonian for the left (right) lead, which includes the coupling to the central region. Assuming that the central sample has  $2L + 1$ , the Hamiltonian of the central region

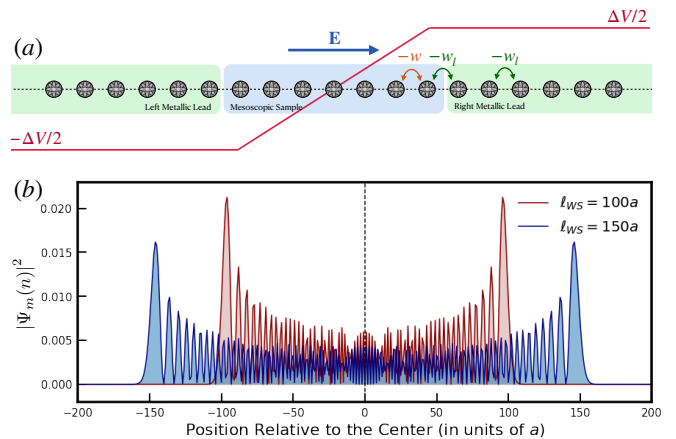


Figure 1. (a) Depiction of the 1D mesoscopic device used throughout this work. The red line represents the spatial profile of the applied electric potential, with  $\Delta V$  being the bias voltage and  $w$  ( $w_l$ ) the hopping parameter inside the central sample (each of the leads). (b) The square-modulus of a Wannier-Stark state [Eq. (5)] centered in site  $m = 0$ ] for two values of the applied electric field (corresponding to  $\ell_{ws} = 100a$  and  $150a$ ).

reads

$$\mathcal{H}_C(t) = \sum_{n=-L}^L V_n^C(t) |n\rangle \langle n| - w \sum_{n=-L}^{L-1} (|n\rangle \langle n+1| + \text{h.c.}), \quad (2)$$

where  $|n\rangle$  describes an electron at position  $n$ ,  $w$  is the nearest-neighbour hopping and  $V_n^C(t) = \Theta(t)eEan$  (with  $a$  the lattice spacing,  $-e$  the electron charge) is the potential due a constant electric field, applied to the central region, that is switched on at  $t = 0$ . The Hamiltonians of the leads read

$$\begin{aligned} \mathcal{H}_L(t) &= \sum_{n=-\infty}^{-L-1} (V_n^L(t) |n\rangle \langle n| - w_l |n+1\rangle \langle n| + \text{h.c.}) \quad (3) \\ \mathcal{H}_R(t) &= \sum_{n=L+1}^{+\infty} (V_n^R(t) |n\rangle \langle n| - w_l |n-1\rangle \langle n| + \text{h.c.}) \end{aligned} \quad (4)$$

where  $w_l$  are the lead hoppings, which unlike in Refs. [40, 51, 54] we will allow to be  $w_l \neq w$ , and  $V_n^L(t) = -\Theta(t)\Delta V/2$ ,  $V_n^R(t) = \Theta(t)\Delta V/2$  are shifts in the local energy of the lead sites, such that no electric field is applied in the leads, with the potential difference related to the electric field in the central region via  $\Delta V = E(2La)$ . The Hamiltonian is illustrated in Fig. 1(a). In numerical simulations, we will actually consider large, but finite leads, instead of semi-infinite ones.

At times  $t > 0$  and in the limit  $L \rightarrow \infty$ , the Hamiltonian  $\mathcal{H}_C(t)$  reduces to the Wannier-Stark Hamiltonian.

It was first shown by G. Wannier<sup>55</sup> that this model has an exact solution consisting of a *Wannier-Stark ladder* spectrum made up of a discrete set of non-degenerate and equally spaced energy levels,  $\varepsilon_m = maeE$ , with  $m \in \mathbb{Z}$ . The corresponding eigenstates are the so-called Wannier-Stark states (WSSs) which, in a real-space representation, are given by<sup>56;57</sup>

$$|\Psi_m\rangle = \sum_{n=-\infty}^{\infty} \psi_m(n) |n\rangle = \sum_{n=-\infty}^{\infty} J_{n-m} \left( \frac{2w}{aeE} \right) |n\rangle, \quad (5)$$

where  $J_n(x)$  are Bessel functions of the first-kind. State  $|\Psi_m\rangle$  is centered at the site  $m$  and has an effective half-width of  $\ell_{\text{WS}} = 2w/(aeE)$ . For  $|n-m| \gg \ell_{\text{WS}}$ , the WSS decay exponentially as  $|\psi_m(n)| \sim e^{-|n-m|/\xi_{\text{WS}}}$ , with  $\xi_{\text{WS}}^{-1} = \log(\ell_{\text{WS}}^{-1})$ . It is important to notice that for strong biases,  $aE \gg w$ , we have that  $\xi_{\text{WS}} \ll \ell_{\text{WS}}$ , meaning that in these conditions the central eigenstates of a finite chain are well approximated by the WSSs of the infinite system. In Appendix A, we review how WSSs give origin to current BOs.

Following a partition-free approach to transport<sup>33</sup>, for times  $t < 0$ , the leads and central region are connected and in thermodynamic equilibrium. The initial state is thus characterized by the reduced density matrix

$$\rho_0 = f(\mathcal{H}_0) = \sum_{\alpha} f(\varepsilon_{0,\alpha}) |\psi_{0,\alpha}\rangle \langle \psi_{0,\alpha}| \quad (6)$$

where  $\varepsilon_{0,\alpha}$  and  $|\psi_{0,\alpha}\rangle$  are the eigenenergies and eigenstates of the initial Hamiltonian  $\mathcal{H}_0 \equiv \mathcal{H}(t < 0)$ .  $f(\varepsilon) = [e^{\beta(\varepsilon-\mu)} + 1]^{-1}$  is the Fermi distribution function, with  $\beta^{-1} = k_B T$  the inverse temperature and  $\mu$  the common Fermi energy. For concreteness, we will assume that the system is initially at half-filling,  $\mu = 0$ , and restrict ourselves to the zero temperature limit. At  $t = 0$ , the electric field is switched on, driving the system away from equilibrium and generating current flow.

## B. Method of Quantum Time-Evolution

Our numerical study simulates the time-dependent charge current that traverses a bond in the system, once the electric field in the central region has been turned on. The local current going from site  $n \rightarrow n+1$  is represented by the operator

$$\mathcal{I}_{n,n+1} = -i(|n+1\rangle \langle n| - |n\rangle \langle n+1|), \quad (7)$$

whose time-dependent expectation value is given by

$$\begin{aligned} I_{n,n+1}(t) &= \text{Tr} [\rho_0 e^{i\mathcal{H}_+ t} \mathcal{I}_{n,n+1} e^{-i\mathcal{H}_+ t}] \\ &= 2\text{Im} \langle n | e^{i\mathcal{H}_+ t} \rho_0 e^{-i\mathcal{H}_+ t} | n+1 \rangle, \end{aligned} \quad (8)$$

Algorithm for Quantum Time-Evolution:

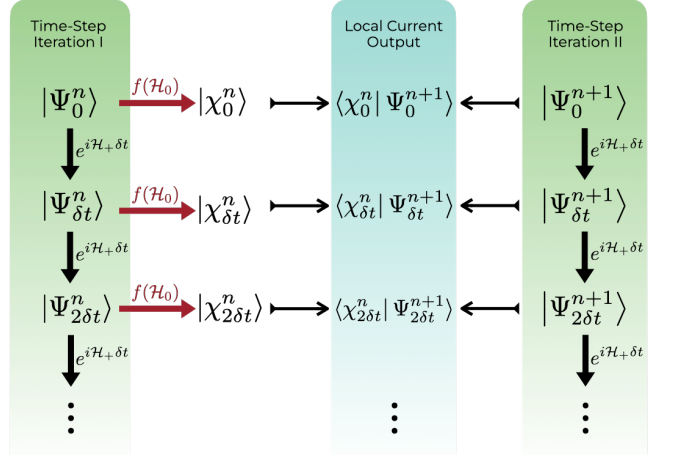


Figure 2. Scheme of the algorithm used to time-evolve the system of Fig. 1.

where  $\rho_0$  is the initial reduced density matrix (6) for the partition-free setup, and  $\mathcal{H}_+ \equiv \mathcal{H}(t > 0)$  is the Hamiltonian after the electric field is turned on, which is constant for  $t > 0$ . By defining

$$|\Psi_t^{n+1}\rangle = e^{-i\mathcal{H}_+ t} |n+1\rangle, \quad (9)$$

$$|\Psi_t^n\rangle = e^{-i\mathcal{H}_+ t} |n\rangle, \quad (10)$$

$$|\chi_t^n\rangle = f(\mathcal{H}_0) |\Psi_t^n\rangle, \quad (11)$$

the expectation value of the current can be written as an inner product

$$I_{n,n+1}(t) = 2\text{Im} \langle \chi_t^n | \Psi_t^{n+1} \rangle. \quad (12)$$

In order to evaluate the current of the system, we will consider finite leads, such that the whole system (central region + leads) has  $N$  sites. As shown by Santos Pires *et al.*<sup>44</sup>, truncation of the leads does not affect the current for times  $t < L_l/w_l$ , where  $L_l$  is the number of sites of the lead, after which effects of electron reflection at the chain boundaries start to manifest. Truncation of the system allows for a simple expansion of the time evolution operator,  $e^{i\mathcal{H}_+ t}$ , and initial reduced density matrix,  $\rho_0 = f(\mathcal{H}_0)$ , in terms of Chebyshev polynomials<sup>58</sup> of  $\mathcal{H}_+$  and  $\mathcal{H}_0$ , respectively. Explicitly we have

$$\exp[-i\mathcal{H}_+ t] \approx \sum_{m=0}^{M_t} \frac{2(-i)^m}{1 + \delta_{m,0}} J_m(\Delta_\epsilon t) T_m\left(\frac{\mathcal{H}_+}{\Delta_\epsilon}\right), \quad (13)$$

$$f(\mathcal{H}_0) \approx \sum_{m=0}^{M_p} \frac{2\mu_m^p}{1 + \delta_{m,0}} T_m\left(\frac{\mathcal{H}_0}{\Delta_\epsilon}\right), \quad (14)$$

where  $\Delta_\epsilon$  is a positive energy scale that normalizes the Hamiltonian spectrum to be within  $[-1, 1]$ ,  $J_m(x)$  is a Bessel function of the first kind,  $T_m(x)$  is a Chebyshev polynomial of the first kind, and  $M_p/M_t$  indicate the

truncation order of each expansion. While the form of the expansion coefficients for the time-evolution operator are known analytically<sup>59</sup>, the values of  $\mu_m^\rho$  must be determined by evaluating the integral

$$\mu_m^\rho = \int_{-1}^1 du \frac{T_m(u)}{\pi \sqrt{1-u^2} [1 + e^{\beta(\Delta_\epsilon u - \mu)}]}, \quad (15)$$

which can be easily done numerically. For times  $t > 0$ , we evaluate the current at discrete mesh of  $N_t$  points —  $\{0, \delta t, 2\delta t, \dots, t_{\max}\}$  — with a time step of  $\delta t = t_{\max}/N_t$ . Therefore, we can write the short time evolution,  $|\Psi_{k\delta t}^n\rangle = e^{-i\mathcal{H}_+\delta t} |\Psi_{(k-1)\delta t}^n\rangle$ ,  $k = 1, \dots, N_t$ , using Eq. (13). The application of  $f(\mathcal{H}_0)$ , in Eq. (11), is implemented using Eq. (14). Crucial for the performance of the method is the fact that it only requires the evaluation of the action of  $e^{-i\mathcal{H}_+\delta t}$  and  $f(\mathcal{H}_0)$  on states  $|\Psi_{k\delta t}^n\rangle$ . When doing so, quantities of the form  $|\Psi_{k\delta t}^n(m)\rangle \equiv T_m(\mathcal{M}) |\Psi_{k\delta t}^n\rangle$ , with  $\mathcal{M} = \mathcal{H}_+/0/\Delta_\epsilon$ , can be efficiently evaluated using the Chebyshev recursion

$$|\Psi_{k\delta t}^n(m+2)\rangle = 2\mathcal{M} |\Psi_{k\delta t}^n(m+1)\rangle - |\Psi_{k\delta t}^n(m)\rangle, \quad (16)$$

starting with  $|\Psi_{k\delta t}^n(0)\rangle = |\Psi_{k\delta t}^n\rangle$  and  $|\Psi_{k\delta t}^n(1)\rangle = \mathcal{M} |\Psi_{k\delta t}^n\rangle$ . Therefore, the method only requires matrix-vector multiplications and has a computational complexity of  $\mathcal{O}(N_t N M_t M_\rho)$ , for sparse Hamiltonians. The implementation scheme is illustrated in Fig. (2).

### III. BLOCH OSCILLATIONS WITHIN A MESOSCOPIC DEVICE

We will start by studying the case when the hopping in the leads and the central region are the same,  $w_l = w$ , a case which was previously discussed by Popescu and Croy<sup>51</sup>. We show the evaluated current for different values of the electric field, measured inside the central region, in the top panel of Fig. 3. For large values of the electric field (small values of  $\ell_{WS}$ ) the current displays an oscillatory behaviour with period  $T_{BO} = 2\pi/(eaE)$ . As the electric field is reduced, the oscillations become deformed (clipped) in time. Finally, we observe that as the electric field is reduced such that  $\ell_{WS} > L$ , the Bloch oscillations disappear and the current tends to a constant value. The current measured in the leads is zero when Bloch oscillations are observed in the central region, as shown in the bottom panel of Fig. 3. When Bloch oscillations are absent, a steady state develops and the current in the leads tends to the same constant value as the current inside the central region. The condition for the observation of BOs,  $\ell_{WS} < L$ , can be interpreted in terms of the localization properties of the WSSs. For strong electric field, the eigenstates of  $\mathcal{H}_+$  will be nearly indistinguishable from the WSSs of an infinite Wannier-Stark chain. Since the current is a local operator, we expect that its expected value will then have the same

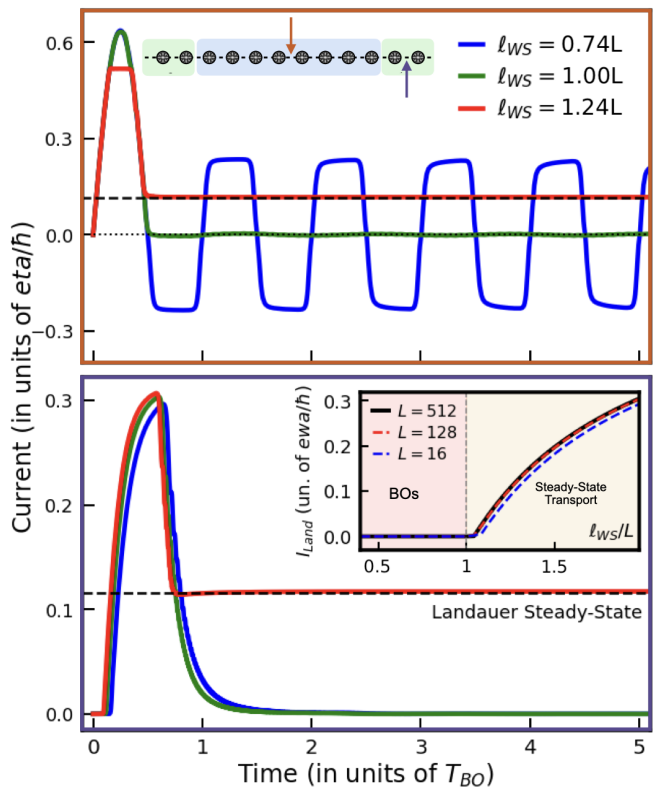


Figure 3. Current in mesoscopic device as a function of time (measured in units of  $T_{BO} = 2\pi/(eaE)$ ) measured inside the central region (top panel), and measured in the right lead (bottom panel), for different values of the electric field in the central region. The dashed lines represent the value of the steady state current, for the cases in which it exists. Inset of bottom panel: Landauer steady-state current as a function of the Wannier-Stark localization length divided by the size of the sample, for various sizes. The vertical dashed line marks the limiting value  $\ell_{WS} = L$ , beyond which a non-zero steady-state current emerges. A central region with 257 sites ( $L = 128$ ), leads with  $L_l = 16000$  sites and  $w_l = w$  was used.

oscillations as the ones of a Wannier-Stark chain. As the electric field is reduced, eigenstates localized at the center of the sample will remain largely unchanged, but the states closer to the edges of the central region will start to leak into the closest lead. As such, these states will not contribute to the Bloch oscillations, which will thus become clipped. Finally, if the bias becomes too small, the most central state of the system will eventually become delocalized, bridging the two leads and carrying a steady-state current. This mechanism is illustrated in Fig. 4(a). Notice that the previous argument does not tell us anything about the value of the current in leads. In particular, it provides no explanation why the current is zero there when BOs occur. In order to do so, we must analyse the spectrum of the leads. The Landauer formula tells us that to obtain a steady-state current we must have an electron in an occupied state of one lead tunneling into an empty state of the other lead. Therefore, the spectrum

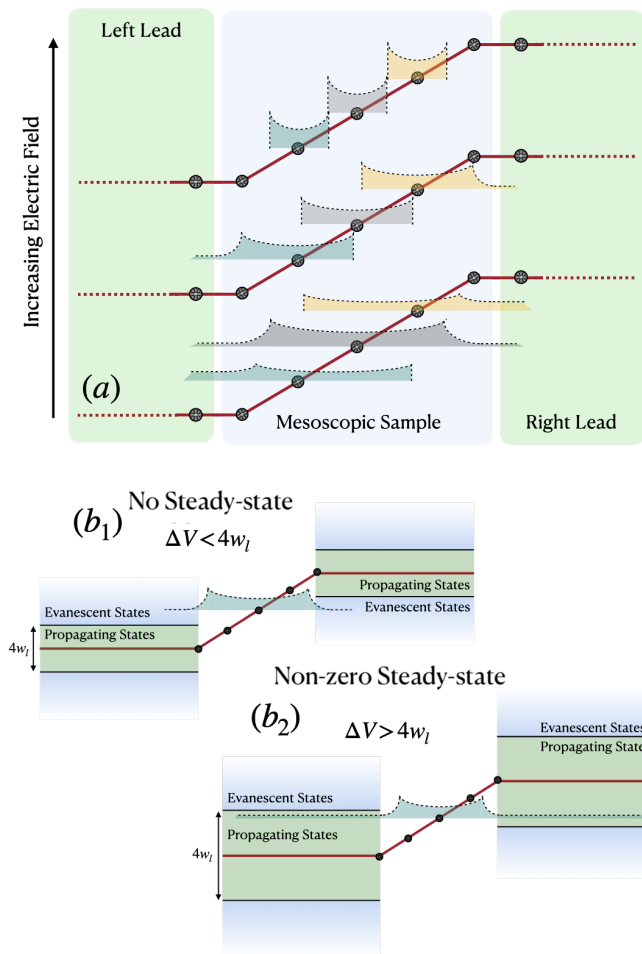


Figure 4. Visualization of the conditions for (a) observation of Bloch oscillations, (b) formation of a non-zero steady state current.

of the leads must overlap in energy. A one dimensional tight-binding model with nearest-neighbour hopping  $w_l$  has a spectrum with a bandwidth of  $4w_l$ . If the leads are half-filled, the spectra of the left and right leads overlap provided  $\Delta V < 4w_l$ , as depicted in Fig. 4(b) and a non-zero steady-state current is possible. If  $\Delta V > 4w_l$ , since there is no overlap between the spectra of the two leads, there is no propagating state that connects both leads and the steady-state current must be zero. In this case, incoming electrons from one lead suffer total reflection as the other lead does not support propagating states at that energy. If  $w_l = w$ , and recalling  $\ell_{\text{WS}} = 2w/(eEa)$ , we have that the condition for the observation of BOs,  $\ell_{\text{WS}} < L$ , coincides with the condition for zero steady-state current,  $\Delta V > 4w$ , a condition previously found by Popescu and Croy<sup>51</sup>. This is in agreement with the results for the steady-state current in Fig. 3, for different central sample sizes and different values of  $\ell_{\text{WS}}$ , obtained using the Landauer formula as implemented in the Kwant package<sup>53</sup>.

The previous discussion makes clear that the simulta-

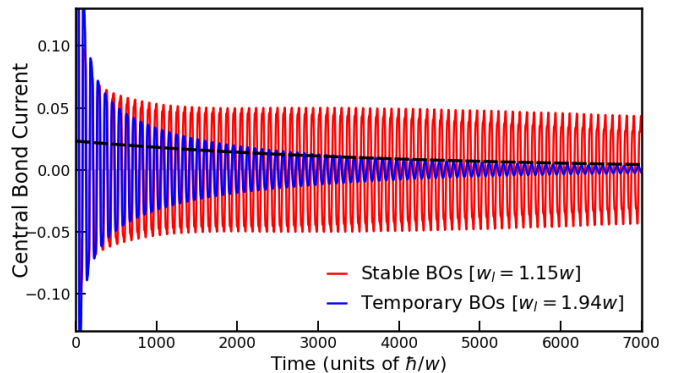


Figure 5. Plots of the local electric current measured over time in the central bond of the mesoscopic sample composed of 69 sites ( $L = 34$ ) and a bias potential  $\Delta V = 5w$ . We showcase two examples of: (i) a mesoscopic device supporting stable clipped BOs if  $w_l = 1.15w$  ( $w_l < \Delta V/4$ ), and (ii) a mesoscopic device having  $w_l = 1.94w$  ( $w_l > \Delta V/4$ ) that now supports tBOs that decay exponentially in time. Such decay is seen to correspond to a decaying time given by  $(1/\tau_0 + 1/\tau_1)^{-1}$  (dashed black line) for long times.

neous observation of BOs in the central region and zero steady-state current in leads is an artifact of having the hoppings in the central region and leads be the same,  $w_l = w$ . Otherwise, the condition for the observation of BOs,  $\ell_{\text{WS}} < L/2 \Leftrightarrow 4w < \Delta V$ , and the condition for observation of a non-zero steady state current,  $\Delta V < 4w_l$ , become distinct. Therefore, if we are in a regime where  $4w < \Delta V < 4w_l$ , we can expect to simultaneously observe BOs and a steady-state non-zero current. Indeed, this is what occurs as can be seen in Fig. 5, where we show the current for a case where  $w_l = w$ , with persistent BOs (a small modulation of the oscillations can be observed, which is discussed in Appendix B) and another with  $w_l \neq w$ , for which BOs acquire a finite lifetime and coexist with a non-zero steady-state current. As an oscillating current precludes the formation of a steady-state, BOs that coexist with a steady-state cannot be persistent and must instead be a transient phenomena with a characteristic decay rate, which we will refer to as transient Bloch Oscillations (tBOs).

#### IV. QUASIPARTICLE APPROXIMATION TO TRANSIENT BLOCH OSCILLATIONS

##### A. Quasiparticle states of the central region

Having established the possibility of transient BOs, we will now develop approximate theory to describe their decay times. Our starting point is the Caroli formula<sup>28</sup>, which expresses the transmittance  $\mathcal{T}(\epsilon)$ , at an energy  $\epsilon$ , in terms of Green's function as

$$\mathcal{T}(\epsilon) = \text{Tr} [\mathbf{G}^\dagger(\epsilon) \cdot \mathbf{\Gamma}_R(\epsilon) \cdot \mathbf{G}(\epsilon) \cdot \mathbf{\Gamma}_L(\epsilon)], \quad (17)$$

where is a trace over the central sample's Hilbert space,  $\mathbf{G}(\epsilon)$  is the retarded Green's function of the central sample when connected to the leads

$$\mathbf{G}(\epsilon) = [\epsilon - \mathbf{H}_C - \Sigma_R(\epsilon) - \Sigma_L(\epsilon)]^{-1}, \quad (18)$$

in terms of the isolated central sample's Hamiltonian  $\mathbf{H}_C$  [Eq. (2) for  $t > 0$ ] and the self-energies introduced by the connected semi-infinite leads,  $\Sigma_{R/L}(\epsilon)$ , and the quantities  $\Gamma_{R/L}(\epsilon) = i[\Sigma_{R/L}(\epsilon) - \Sigma_{R/L}^\dagger(\epsilon)]$ , are the *level-width matrices*. For semi-infinite tight-binding chains, one can analytically determine the self-energy, thus arriving at the expressions <sup>44;60</sup>,

$$\Sigma_{R/L}(\epsilon) = w_l \Sigma \left( \frac{\epsilon \pm \Delta V/2}{2w_l} \right) |\pm L\rangle \langle \pm L| \quad (19)$$

where  $\Sigma(\epsilon) = \epsilon - i\sqrt{1 - (\epsilon + i0^+)^2}$ . The Green's function of the central region  $\mathbf{G}(\epsilon)$  can be expressed in terms of its right,  $|\Phi_n^R(\epsilon)\rangle$ , and left,  $\langle \Phi_n^L(\epsilon)|$ , eigenvectors of the effective (non-hermitian) Hamiltonian of the central region connect to the leads,  $\mathcal{H}_{\text{eff}}(\epsilon) = \mathbf{H}_C + \Sigma^R(\epsilon) + \Sigma^L(\epsilon)$ .<sup>61</sup> We have that

$$\mathbf{G}(\epsilon) = \sum_n \frac{|\Phi_n^R(\epsilon)\rangle \langle \Phi_n^L(\epsilon)|}{\epsilon - \epsilon_n(\epsilon) + i\gamma_n(\epsilon)}, \quad (20)$$

where the summation is over the entire Hilbert space of the central sample, and  $\epsilon_n(\epsilon) - i\gamma_n(\epsilon)$  are the eigenvalues of  $\mathcal{H}_{\text{eff}}(\epsilon)$ , separated into their real and imaginary parts. Notice that both the eigenvectors,  $|\Phi_n^R(\epsilon)\rangle$  and  $\langle \Phi_n^L(\epsilon)|$ , and the eigenvalues,  $\epsilon_n(\epsilon) - i\gamma_n(\epsilon)$ , are a function of the energy  $\epsilon$ .

If the states of the central region are only weakly perturbed by the hybridization with the leads, the eigenvalues,  $|\Phi_n^{R/L}(\epsilon)\rangle$ , and eigenstates,  $\epsilon_n(\epsilon) - i\gamma_n(\epsilon)$ , will be weakly dependent on the energy  $\epsilon$ . Furthermore, if the electric field is strong enough,  $\ell_{\text{WS}} \ll L$ , the eigenstates and eigenvalues of  $\mathcal{H}_{\text{eff}}(\epsilon)$  will be well approximated by WSS. We will refer to these approximations as the *weak coupling and strong field approximation*. With these considerations, we can employ a quasiparticle approximation (QPA) to the Green's function,  $\mathbf{G}(\epsilon)$ , in which we approximate  $|\Phi_n^{R/L}(\epsilon)\rangle \simeq |\Phi_n^{R/L}(\epsilon_{c,n})\rangle \equiv |\Phi_{n,\text{QPA}}^{R/L}\rangle$  and  $\epsilon_n(\epsilon) - i\gamma_n(\epsilon) \simeq \epsilon_n(\epsilon_{c,n}) - i\gamma_n(\epsilon_{c,n}) \equiv \epsilon_n^{\text{QPA}} - i\gamma_n^{\text{QPA}}$ , where  $\epsilon_{c,n}$  are the eigenstates of the isolated central region,  $\mathbf{H}_C$ .<sup>62</sup> Therefore,  $\epsilon_n(\epsilon_{c,n})$  are the corrected energy levels and  $\gamma_n(\epsilon_{c,n})$  the corresponding broadenings or decay rates induced by the hybridization of the central region with the leads. Within the QPA we have that

$$\mathbf{G}(\epsilon) \simeq \mathbf{G}_{\text{QPA}}(\epsilon) = \sum_n \frac{|\Phi_{n,\text{QPA}}^R\rangle \langle \Phi_{n,\text{QPA}}^L|}{\epsilon - \epsilon_n^{\text{QPA}} + i\gamma_n^{\text{QPA}}}. \quad (21)$$

Within the weak coupling and strong field approximations, we also have that  $|\epsilon_n^{\text{QPA}} - \epsilon_{n+1}^{\text{QPA}}| \gtrsim$

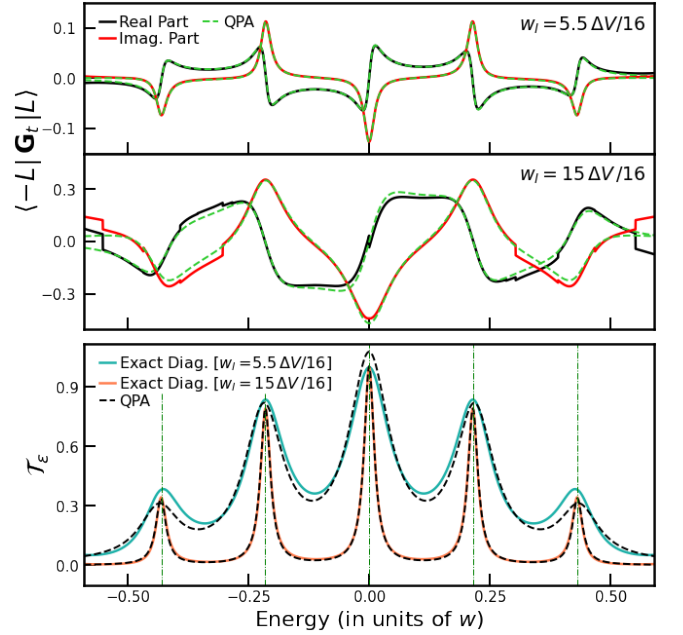


Figure 6. Top panel: real and imaginary parts of the the Green's function  $\langle -L | \mathbf{G}(\epsilon) | L \rangle$  as a function of energy for a system with  $L = 12$ ,  $\Delta V = 4.3w$  and two values of  $w_l$ . The full lines represent exact results and the dashed lines represent results obtained within the QPA. Bottom panel: transmittance  $\mathcal{T}(\epsilon)$  as a function of energy, for the same system as in the top panel. The vertical lines, represent the energies of the inner most WSS,  $\epsilon_m = eEam$ ,  $m = 0, \pm 1, \pm 2$ .

$\gamma_n^{\text{QPA}}, \gamma_{n+1}^{\text{QPA}}$ , which allows us to further approximate the transmission, which can be written as  $\mathcal{T}(\epsilon) = \Gamma_L(\epsilon)\Gamma_R(\epsilon)|\langle -L | \mathbf{G}(\epsilon) | L \rangle|^2$ , as a sum of Lorentzians

$$\begin{aligned} \mathcal{T}(\epsilon) &\simeq \mathcal{T}_{\text{QPA}}(\epsilon) \\ &= \Gamma_L(\epsilon)\Gamma_R(\epsilon) \sum_n \frac{|\langle L | \Phi_{n,\text{QPA}}^R \rangle|^2 |\langle \Phi_{n,\text{QPA}}^L | -L \rangle|^2}{(\epsilon - \epsilon_n^{\text{QPA}})^2 + (\gamma_n^{\text{QPA}})^2}, \end{aligned} \quad (22)$$

where  $\Gamma_{L/R}(\epsilon) = \sqrt{(2w_l)^2 - (\epsilon \pm \Delta V/2)^2}$ . In Fig. 6, we show the real and imaginary parts of  $\langle -L | \mathbf{G}(\epsilon) | L \rangle$  and of the transmission computed both exactly and within the QPA. The exact results for the transmittance were obtained using the *Kwant* package<sup>53</sup>. We can see that the QPA works remarkably well, provided we are in the conditions for strong field and weak coupling, ( $\ell_{\text{WS}} \ll L$ ), for the most central states of the device (which are the least hybridized with the leads). We can see that the transmittance indeed approaches a sum of Lorentzian functions centered at the QPA energies  $\epsilon_n^{\text{QPA}}$  and with width given by  $\gamma_n^{\text{QPA}}$ . As we will see in the next subsection, the decay rate of the tBOs are related to  $\gamma_n^{\text{QPA}}$ . Interestingly, we see that the width of the Lorentzians reduces with and increasing  $w_l$ .

## B. Transient current due to quasiparticle states

We will now develop a time-resolved theory for tBOs based on the QPA. We will start by arguing that the tBO are a phenomena that depends on the local properties of the central region that is subjected to the electric field. This is illustrated by the results of Fig. 3, where we can see that BOs can be observed in the current measured in the central region, but not on the leads. Furthermore, we know that the steady-state current depends only on the occupation of the leads, with effects due to the occupation of the central region being washed-out. Therefore, this further reinforces the notion that tBO depend mostly on the occupation of states in the central region. Therefore, we approximate the current measured in the central region as

$$I_{n,n+1}(t) \simeq I_{\text{Land}} + I_{n,n+1}^{\text{Trans}}(t), \quad (23)$$

where  $I_{\text{Land}}$  is the Landauer steady-state current, which is controlled by the occupation of the leads, and

$$I_{n,n+1}^{\text{Trans}}(t) = \hbar^2 \text{Tr} [\rho_{C,0} \mathbf{G}^\dagger(t) \mathcal{I}_{n,n+1} \mathbf{G}(t)] \quad (24)$$

approximates the current due to the occupation of the central region, which will capture the tBO. In the above expression  $\rho_{C,0}$  is the projection of the initial (partition-free) reduced density matrix onto the central region, and  $\mathbf{G}(t)$  is the projection of the full time evolution operator  $e^{-\frac{i}{\hbar} \mathcal{H}t}$  into the central region, which is nothing more than the retarded Green's function of the central region. Within the QPA, we use Eq. (21), which leads to

$$\begin{aligned} \mathbf{G}(t) &= \int \frac{d\epsilon}{2\pi\hbar} e^{-i\epsilon t/\hbar} \mathbf{G}(\epsilon) \\ &\simeq -\frac{i}{\hbar} \Theta(t) \sum_n e^{-i(\epsilon_n^{\text{QPA}} - i\gamma_n^{\text{QPA}})t/\hbar} |\Phi_{n,\text{QPA}}^R\rangle \langle \Phi_{n,\text{QPA}}^L|. \end{aligned} \quad (25)$$

We therefore, obtain the approximate equation for the transient current inside the central region

$$\begin{aligned} I_{n,n+1}^{\text{Trans}}(t) &\simeq \sum_{m,r} e^{-(\gamma_m^{\text{QPA}} + \gamma_r^{\text{QPA}})t/\hbar} e^{-i(\epsilon_m^{\text{QPA}} - \epsilon_r^{\text{QPA}})t/\hbar} \times \\ &\times \langle \Phi_{m,\text{QPA}}^L | \rho_{C,0} | \Phi_{r,\text{QPA}}^L \rangle \langle \Phi_{r,\text{QPA}}^R | \mathcal{I}_{n,n+1} | \Phi_{m,\text{QPA}}^R \rangle. \end{aligned} \quad (26)$$

In Fig. (7), we compare the exact result of the time-resolved current with the estimation of the transient current within the QPA. We see that for large enough times we obtain an excellent agreement. For shorter times we see significant differences. We attribute these differences to the fact that at short time scales, the current will be dominated by states strongly hybridized with the leads, for which the QPA fails. For large enough times, the decay of the tBOs is well approximated by a single exponential. To estimate its effective decay time, we

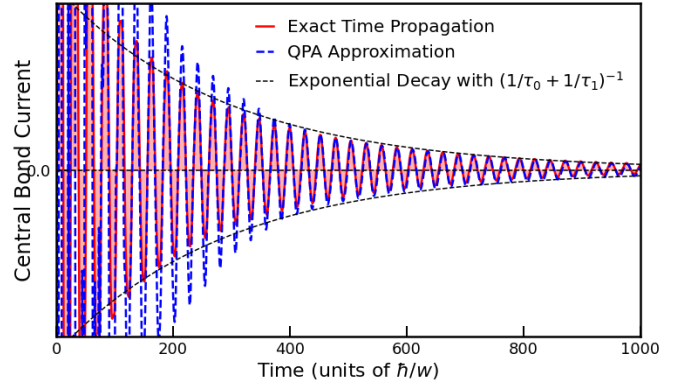


Figure 7. Current measured in the central region computed exactly (solid, red line) and within the QPA (dashed, blue line) [Eq. (26)].

first notice that deep inside the central region, the quasiparticle eigenstates are well approximated by the WSS, which are purely real, which allow us to conclude that  $\langle \Phi_{m,\text{QPA}}^R | \mathcal{I}_{n,n+1} | \Phi_{m,\text{QPA}}^R \rangle \simeq 0$ . In addition, we also expect the inner most states of the central region will have the smallest decay rates, as these are more weakly coupled to the leads. Finally, the diagonal contributions to the transient current in equation 26 will not contribute with an oscillatory dynamic, since the power of the complex exponential will vanish for these terms. For these reasons, we conclude that for relatively long times, the sum in Eq. (26) will be dominated by the contributions from  $(m,r) = (0,\pm 1), (\pm 1,0)$ , which leads to an effective decay time for the tBOs of  $\tau_{\text{eff}} = (\gamma_0^{\text{QPA}} + \gamma_1^{\text{QPA}})^{-1}$ , where we used the fact that  $\gamma_1^{\text{QPA}} = \gamma_{-1}^{\text{QPA}}$ . As shown in Figs. 5 and 7, the decay of the tBO for large times is well captured by  $\tau_{\text{eff}}$ .

## C. Quasianalytic estimation of the tBO decay time

We will now provide a quasianalytic expression for the decay time of the inner most quasiparticle states of the central region. To do so, we start by noticing that within the QPA the decay rates can be approximated by

$$\gamma_n^{\text{QPA}} \simeq -\text{Im} \langle \Phi_{n,\text{QPA}}^L | \Sigma_{\text{R}}(\epsilon_{C,n}) + \Sigma_{\text{L}}(\epsilon_{C,n}) | \Phi_{n,\text{QPA}}^R \rangle. \quad (27)$$

In the previous equation, we might be tempted to further approximate the quasiparticle states by the WSS. However, even though the quasiparticle eigenstates are well approximate by WSS deep within the central region, closer to the edges significant differences can be observed. We make instead the following ansatz

$$\gamma_n^{\text{QPA}} \simeq -\frac{1}{C_n(w_l, \Delta V)} \text{Im} \langle \Psi_n | \Sigma_{\text{R}}(\epsilon_{C,n}) + \Sigma_{\text{L}}(\epsilon_{C,n}) | \Psi_n \rangle, \quad (28)$$

where  $|\Psi_n\rangle$  are the WSS [Eq. (5)] and we assumed that  $C_n(w_l, \Delta V)$  is independent of the central region size. We

can now evaluate analytically

$$\begin{aligned} & \text{Im} \langle \Psi_n | \Sigma_R(\epsilon_{C,n}) + \Sigma_L(\epsilon_{C,n}) | \Psi_n \rangle = \\ & = \frac{1}{2} \Gamma_L(\epsilon_{C,n}) J_{L+n}^2(\ell_{\text{WS}}) + \frac{1}{2} \Gamma_R(\epsilon_{C,n}) J_{L-n}^2(\ell_{\text{WS}}). \end{aligned} \quad (29)$$

To make progress, we recall that the QPA is only valid in the strong field and weak coupling limit,  $\ell_{\text{WS}} \ll L$ . Furthermore, we will focus on the decay rate of the three innermost states,  $n = 0, \pm 1$ , which dominate the decay rate of the tBOs for long enough times. Specializing to  $n = 0, \pm 1$  in the limit  $\ell_{\text{WS}} \rightarrow 0^+$ , we approximate  $\Gamma_L(\epsilon_{C,n}) \simeq \Gamma_R(\epsilon_{C,n}) = \sqrt{4w_l^2 - \Delta V^2} + \mathcal{O}(n/L)^2$  and approximate the Bessel functions as (see Abramowitz and Stegun<sup>63</sup>):

$$J_{L+n}(\ell_{\text{WS}}) \simeq \frac{1}{\sqrt{2\pi(L+n)}} \left( \frac{e\ell_{\text{WS}}}{2(L+n)} \right)^{L+n}. \quad (30)$$

We therefore obtain the approximate expression for the decay times

$$\begin{aligned} \frac{\tau_n^{\text{QPA}}}{4\pi} &= \frac{1}{4\pi} \frac{1}{\gamma_n^{\text{QPA}}} \simeq \\ &\simeq \frac{C_n(\delta, \Delta V)(L - |n|)}{(2 - \delta_{0n})\sqrt{\delta(\delta + 2)}} \left[ \frac{L - |n|}{4e(L + 1)} \right]^{2(L - |n|)} \Delta V^{2(L - |n|) - 1}, \end{aligned} \quad (31)$$

where we introduced the parameter  $\delta = 4w_l/\Delta V - 1$  that describes the overlap between the bands of propagating states in both leads. Note that tBOs only exist if  $\delta > 0$  and, as shown in Eq. (31), the lifetimes associated to the central most WSSs of the mesoscopic sample diverge as  $\delta \rightarrow 0^+$ . At the same time, we were able to extract analytically that  $\tau_n^{\text{QPA}}$  has a very steep power-law dependence on the bias potential, with an exponent that grows linearly with the sample size. Note that this is a consequence of the exponential tails of the WSSs which, if  $\ell_{\text{WS}} \ll L$ , fully determine the way in which they are affected by the presence of the leads. We assume that  $C_n(\delta, \Delta V) = A_n(\delta + 1)^2 \Delta V^{\nu_n}$ ,  $A_n$  and  $\nu_n$  depend only on  $n$  and can be determined to fit the numerical data (this assumption is numerically validated in Appendix (C)). Note that the dependence of  $\tau_n^{\text{QPA}}$  on the parameter  $\delta$  is fully fixed, which is to say that the dependence on  $w_l$  is completely determined. Furthermore, the extra power law dependence on  $\Delta V$  coming from  $C_n(\delta, \Delta V)$  is much weaker than the one coming from equations (29) and (30), as the coefficients  $\nu_n$  were determined to be 0.41 and 0.28 for  $n = 0, 1$  respectively. We cannot say if the correction coming from the functions  $C_n(\delta, \Delta V)$  to the overall dependence of equation 31 on  $\Delta V$  is truly a power law or a logarithmic correction, since we have not probed these functions with a large enough  $\Delta V$  interval. Nevertheless, this should not matter in the limit of large  $L$ , as this correction is dominated by the power-law that

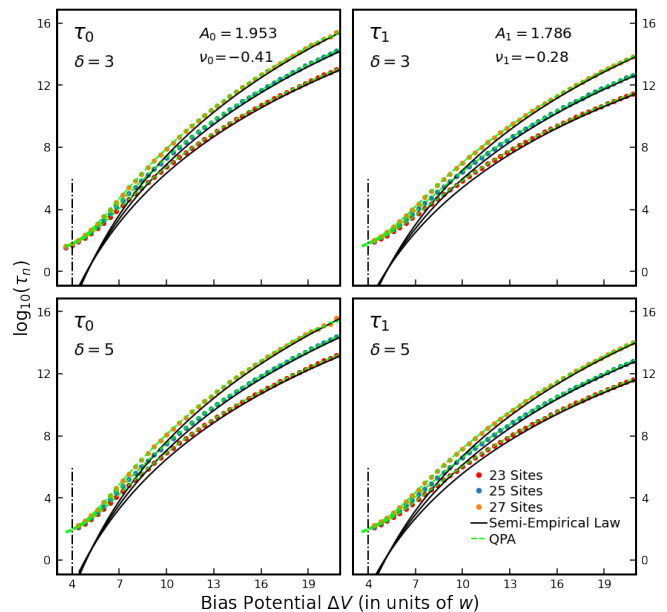


Figure 8. Lifetimes of the WSSs centered on the central ( $\tau_0$ ) and first off-center sites ( $\tau_1 = \tau_{-1}$ ) of the mesoscopic sample, as a function of the potential bias  $\Delta V$ . The dots mark the numerical values extracted from the HWHW of the central lorentzian in quantum transmittance of the biased central sample. Two mesoscopic devices are considered, having  $\delta = 3$  (upper panels) and  $\delta = 5$ , with the black lines representing a fit of the numerical data to the semi-empirical expressions of Eq. (31). The corresponding values of  $A_n$  and  $\nu_n$  are shown in the panels.

comes from equation 29. In Fig. 8 we compare this semi-analytic expression with results obtained within the fully numeric QPA and those obtained by fitting Lorentzian functions to the calculated transmission function for  $\tau_0$  and  $\tau_1$ .

#### D. Numerical extraction of decay times

Having devised a theoretical model to analyze the decaying current oscillations in the strong field and weak coupling regime, we are now in position to complete the analysis of the numerical simulation results first shown in Fig. 5. In Fig. 9(a), we show results for the time-dependent current crossing the central bond of a mesoscopic sample (25 sites) subject to different potential biases,  $\Delta V$ . In all the case, the bandwidths of the leads was adjusted such that  $\delta = 4w_l/\Delta V - 1 = 0.25$  remains constant, thus guaranteeing the existence of tBOs in the central sample. Firstly, we see that in all cases the current displays damped oscillations that decay towards a constant value after a few periods of oscillation. By applying the two-terminal Landauer formula, we further conclude that the asymptotic current corresponds to the Landauer current,  $I_{\text{Land}}$ , of each strongly biased sample. Secondly, we also observe that the decay time of these oscillations



(as well as the pseudo-period) increase with  $\Delta V$  as expected from our theoretical understanding of this phenomenon. In fact, as depicted in the inset of Fig. 9(a), a rescaling of the time variable by the corresponding  $\tau_{\text{eff}}$  serves to collapse the decaying envelope of all the curves, which proves that this is the indicated time-scale.

While the previous analysis seemingly demonstrated that our theoretical model for the tBOs serves to explain the behavior of the current inside a strongly biased mesoscopic sample, we can perform a more precise analysis of the current oscillations in Fig. 9(a). We will focus on the current measured at the center of the sample between sites 0 and 1,  $I_{0,1}(t)$ . For that purpose, we begin by Fourier transforming  $I_{0,1}(t)$  into the frequency-domain ( $\omega$ -domain) which gives rise to the data points plotted in Figs. 9(b). If our model for the tBOs is accurate, then the local current at the center of the sample for long enough times, as per equations 8 and 26, is given by

$$I_{0,1}(t \gg 0) \simeq A \cos(\Omega t + \phi) e^{-t/\tau_{\text{eff}}} + I_{\text{Land}} \quad (32)$$

which, upon removal of the corresponding asymptotic Landauer current, should give rise to the following complex components of the Fourier transform:

$$\text{Re}[I_{0,1}(\omega)] = A\tau_{\text{eff}} \frac{\cos \phi + \tau_{\text{eff}} \sin \phi (\omega - \Omega)}{1 + \tau_{\text{eff}}^2 (\omega - \Omega)^2} \quad (33)$$

$$\text{Im}[I_{0,1}(\omega)] = A\tau_{\text{eff}} \frac{\sin \phi - \tau_{\text{eff}} \cos \phi (\omega - \Omega)}{1 + \tau_{\text{eff}}^2 (\omega - \Omega)^2}. \quad (34)$$

Having Eqs. (33)-(34) as a template, we can now find the values of  $\Omega$  and  $\tau_{\text{eff}}$  by fitting the numerical data for  $I_{0,1}(\omega)$  to these expressions. The corresponding fits are presented in Fig 9(b) and the values of  $\Omega$  and  $\tau_{\text{eff}}$  acquired for various biases are shown in the panels of Fig 9(c). From the presented results it is clear that: (i) the oscillating current is very well described as a single-frequency oscillation with an exponentially decaying envelope, and (ii) the values obtained for the oscillation frequency and decay time perfectly agree with the theoretical predictions of our strong bias model, i.e.,  $\Omega = 2\pi/T_{\text{BO}}$  and  $\tau_{\text{eff}} = \tau_0\tau_1/(\tau_0 + \tau_1)$ .

## V. CONCLUSIONS AND OUTLOOK

We have demonstrated how Bloch oscillations can coexist with the formation of a steady-state current in biased mesoscopic devices. Contrasting with Bloch oscillations in the Wannier-Stark model, these oscillating current acquire a finite lifetime, due to the hybridization to the device leads, and dub them transient Bloch oscillations.

We performed a theoretical analysis of the occurrence of current Bloch oscillations in a « one-dimensional mesoscopic system in a two-terminal configuration. We focused on a nearest-neighbour tight-binding model, with

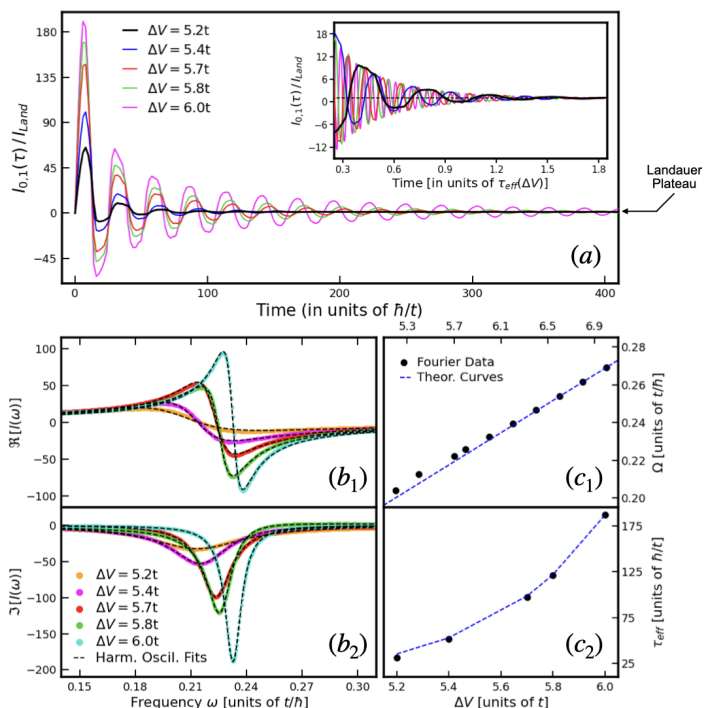


Figure 9. a) Average current evolution divided by the respective Landauer value for different potential biases (in units of  $w$ ) for a sample of size 25 ( $L = 12$ ). b) Same current evolutions with time scaled by the inverse of HWHM coefficients and amplitudes adjusted. The dashed brown line denotes Current/Landauer = 1. b1) Real and b2) complex part of the Fourier transform of the current for different potential biases (in units of  $w$ ) for a system of size 25 ( $L = 12$ ). The dashed lines are the corresponding fits of the functions in Eqs. (33) and (34). c1)  $\Omega$  values obtain from the fit for different  $\Delta V$  (blue points) compared to the frequency of BOs for the corresponding  $\Delta V$  (dashed blue line). c2)  $\tau_{\text{eff}}$  values obtain from the fit for different  $\Delta V$  (blue points) compared to the corresponding values of  $\tau_0\tau_1/(\tau_0 + \tau_1)$  (dashed blue lines).

a partition-free initial condition and at half-filling, with a constant electric field applied to its central region. We conclude that Bloch oscillations can be observed provided  $\ell_{\text{WS}} < La$ , where  $\ell_{\text{WS}} = 2w/(eEa)$  is the localization length of WSS, with  $w$  nearest-neighbour central region hopping and  $E$  the electric field that is applied to a region of length  $(2L+1)a$ . In terms of applied bias voltage, this condition is equivalent to  $\Delta V > 4w$ . If the hopping in the leads is the same as the hopping in the central region, the spectral bandwidth of the leads is  $4w$ , and the condition  $\Delta V > 4w$  implies that no steady-state current can emerge, as previously found<sup>51</sup>. In this regime, no current carrying scattering states can be constructed, and bound states localized in the central region are observed. These bound states are similar to the Wannier-Stark states of an infinite chain subject to a constant electric field. For  $\Delta V < 4w$ , a brief build-up transient is followed by the emergence of a ballistic steady-state Landauer current that flows through the device, but no Bloch oscillations

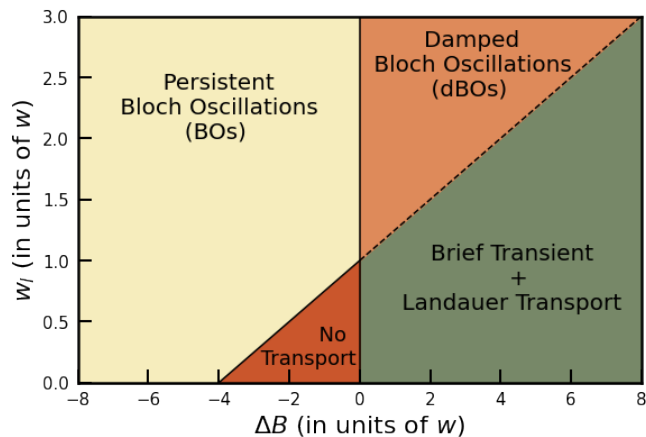


Figure 10. Diagram that summarizes the four different dynamical phases of the strongly biased mesoscopic device, as a function of the relative bandwidth of the leads,  $w_l$ , and the overlap between the bands,  $\Delta B = \delta \times \Delta V$ . Four non-equilibrium regimes are identified: (i) persistent in-sample BOs, (ii) tBOs [decaying towards a Landauer steady-state current after, at least one Bloch period], (iii) a Landauer transport steady-state, and (iv) a regime of blocked transport (with a chaotic current inside the sample).

are observed.

The aforementioned scenario in which Bloch oscillations and Landauer steady-state transport are mutually exclusive quantum transport processes gets drastically changed once the leads are permitted to have a wider bandwidth than the sample. In particular, if the hoppings in the leads,  $w_l$ , differs from the hoppings in the central region,  $w$ , it is possible to observe the coexistence of Bloch oscillations with the formation of a steady-state current provided  $4w < \Delta V < 4w_l$ . In this regime no true bound states localized in the central region exist. Instead, we have quasiparticle states, that resemble Wannier-Stark states, but with a finite lifetime. As such, Bloch oscillations exist as a transient phenomena, decaying in time until a constant and non-zero steady-state current is formed. Crucially, these transient Bloch oscillations display the same frequency of Bloch oscillations in a Wannier-Stark ladder. Numerical simulations based on the unitary time-evolution of the local electric current in a system coupled to finite leads, in conjunction with a quasiparticle approximation scheme, were used to demonstrate the validity of these claims. The *phase diagram* of Fig. 10, which depicts the various dynamical phases of the mesoscopic device as a function of the relative bandwidth of the leads ( $w_l$ ) and the overlap between the bands ( $\Delta B = 4w - \Delta V$ ) summarizes the results.

To summarize, we have found a new regime in which Bloch oscillations can be observed as a transient phenomena in biased mesoscopic systems. These Bloch oscillations could potentially be detected by the radiation emitted by the oscillating current.

## ACKNOWLEDGMENTS

Work supported by the Portuguese Foundation for Science and Technology (FCT) within the Strategic Funding UIDB/04650/2020 and through projects No. POCI-01-0145-FEDER-028887 (J.P.S.P., S.M.J and J.M.V.P.L.), No. CEECIND/02936/2017 and No. EXPL/FIS-MAC/0953/2021 (B.A.). J.P.S.P. and S.M.J are funded by FCT grants No. PD/BD/142774/2018 and PD/BD/142798/2018, respectively.

## Appendix A: Bloch Oscillations and the Wannier-Stark States

At the start of Sec. II, we revised essential aspects of the exact solution for the tight-binding chain subject to an uniform electric field. This turned out to be a crucial theoretical cornerstone for our study because the shape of the WSSs greatly aided in our comprehension of the various regimes of current dynamics in a strongly biased mesoscopic device. We did not, however, fully examine all ramifications of this exact solution, particularly how it relates to the presence of Bloch oscillations in this model. For the sake of completeness, we provide more thorough discussion in this appendix, referring to Hartmann *et al.*<sup>64</sup> for an in-depth approach.

Like before, we start from the Hamiltonian of the system in the presence of a longitudinal electric field  $E$ , which reads,

$$\mathcal{H}_{\text{WS}} = \sum_{n=-\infty}^{+\infty} (-w|n\rangle\langle n+1| + |n+1\rangle\langle n| + aeEn|n\rangle\langle n|), \quad (\text{A1})$$

$|n\rangle$  being local orbitals,  $w$  the nearest-neighbor hopping, and  $a$  the lattice parameter. We have seen that the spectrum of  $\mathcal{H}_{\text{WS}}$  forms a so-called *Wannier-Stark ladder* with discrete energy levels,  $\varepsilon_m = maeE$  (for  $m \in \mathbb{Z}$ ), and that the corresponding eigenstates are localized wavefunctions in real-space [quoted in Eq. (5)]. In place of repeating the real-space representation, we now highlight that the WSSs can also be nicely represented in momentum space as follows<sup>64</sup>:

$$|\Psi_m\rangle = \sqrt{\frac{a}{2\pi}} \sum_k \exp \left[ -iamk + \frac{2w}{iaeE} \sin ka \right] |\phi_k\rangle, \quad (\text{A2})$$

where  $|\phi_k\rangle$  are the lattice momentum eigenstates with  $-\pi \leq ka < \pi$ . Using the eigenstates of the full Hamiltonian, we can write down the exact time-evolution operator,

$$\mathcal{U}(t) = \int_{-\frac{\pi}{a}}^{\frac{\pi}{a}} dk \exp \left[ \frac{2w}{iaeE} \sin \left( ka - \frac{eaEt}{\hbar} \right) \right] \times \exp \left[ -\frac{2w}{iaeE} \sin ka \right] |\phi_{k-eEt/\hbar}\rangle \langle \phi_k|, \quad (\text{A3})$$

where  $t$  is the time parameter, and which can now be used to determine the dynamics of any quantum state in which this system may start. For example, if it starts from a thermal state, in the absence of the electric field, as described by the reduced density matrix

$$\rho_0 = \int_{-\frac{\pi}{a}}^{\frac{\pi}{a}} dk f(\varepsilon_k) |\phi_k\rangle \langle \phi_k|, \quad (\text{A4})$$

where  $f(\varepsilon)$  is the Fermi-Dirac distribution function, and  $\varepsilon_k = -2w \cos ka$  are the energy eigenvalues if  $E = 0$ . In such a case, the time-dependent expectation value of the total electric current operator,

$$\mathcal{I} = \frac{2eaw}{\hbar} \int_{-\frac{\pi}{a}}^{\frac{\pi}{a}} dk \sin ka |\phi_k\rangle \langle \phi_k|, \quad (\text{A5})$$

explicitly yields,

$$J(t) = \text{Tr} [\rho_0 \mathcal{U}(t) \mathcal{I} \mathcal{U}^\dagger(t)] = -\frac{ea}{\hbar} \sin \left( \frac{eEat}{\hbar} \right) \int_{-\frac{\pi}{a}}^{\frac{\pi}{a}} dk f(\varepsilon_k) \varepsilon_k. \quad (\text{A6})$$

Surprisingly, Eq. (A6) demonstrates that, upon the application of an uniform and static electric field, the electric current oscillates in time with a period,

$$T_{\text{BO}} = \frac{2\pi\hbar}{aeE}, \quad (\text{A7})$$

that is inversely proportional to the applied electric field.

## Appendix B: Appearance of a Beat Pattern in Bloch Oscillations

In figure (5) we showcased stable BOs and tBOs by changing the leads hoppings appropriately. For the sake of brevity, we have omitted another effect from the main text, which we will explain in this appendix instead. By setting  $w_l = w$ , the originated BOs display a beat. This effect points to the introduction of new time scales other

than the Bloch period  $T_{\text{BO}}$ . Such time scales appear due to the shift in the energy of the states centered near the boundaries of the sample. This shifts makes it so that the energetic difference between neighbouring states is no longer equal to a multiple of  $eEa$ . However, by increasing  $w_l$ , we can get these states to couple to propagating ones in the leads, thereby allowing them to escape the sample and making them not contribute to the central current. Thus, setting  $w_l$  to a sufficient high value but still below  $\Delta V/4$  shall eliminate the beat while maintaining the BOs stable. In figure (11) we show the central current evolution for three different values of  $w_l$  below the tBO threshold  $\Delta V/4$ :  $0.8w$ ,  $w$  and  $1.15w$ . We notice that the beat is suppressed with the increase of  $w_l$ , corroborating our hypothesis.

## Appendix C: Study of Functions $C_n(\delta, \Delta V)$

In subsection (IV C), we have said that the functions  $C_n(\delta, \Delta V)$  have a fixed dependence on  $\delta$ , a weak power law dependence on  $\Delta V$  and do not depend on  $L$ . To back our claim, we plot these functions for different values of  $L$ ,  $\delta$  and  $\Delta V$  in figure (12). It is clear that these functions do not in fact depend on  $L$  and their behavior is congruent with universal curves of the form  $C_n(\delta, \Delta V) = A_n(\delta + 1)^2 \Delta V^{\nu_n}$ . The coefficients  $A_n$  and  $\nu_n$  are obtained from these plots.

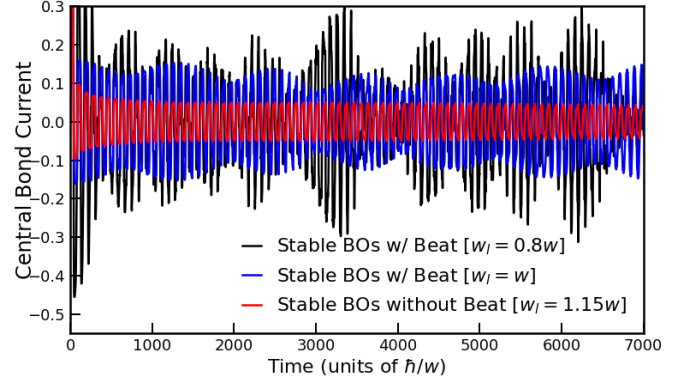


Figure 11. Plots of the local electric current measured over time in the central bond of the mesoscopic sample composed of 69 sites ( $L=34$ ) and a bias potential  $\Delta V=5w$ . We showcase three examples of: (i) a mesoscopic device supporting stable clipped BOs displaying a beat pattern with  $w_l=0.8w$  (ii) a mesoscopic device supporting stable clipped BOs displaying a beat pattern with  $w_l=w$  and (iii) a mesoscopic device supporting stable clipped BOs with no beat pattern with  $w_l=1.15w$ .

[1] F. Bloch, *Z. Physik* **52**, 555 (1929).

[2] C. Zener, *Proc. R. Soc. Lond.* **145**, 523 (1934).

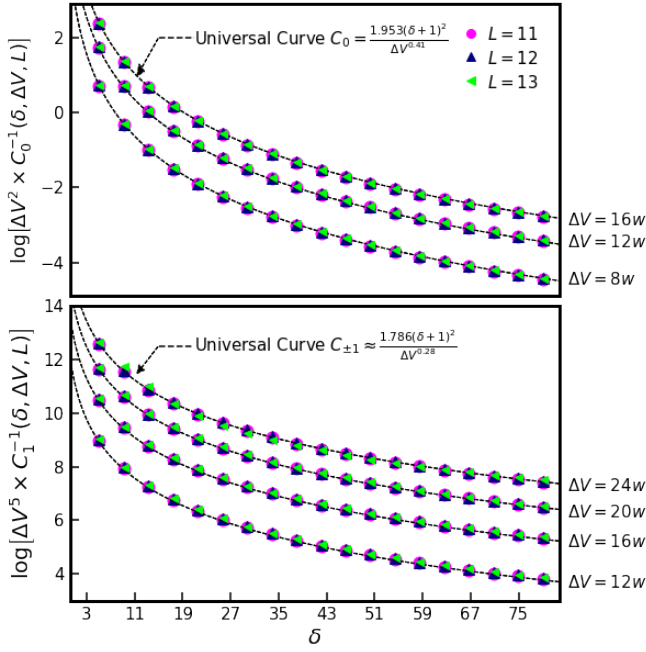


Figure 12. Plots of the inverse of the functions  $C_0(\delta, \Delta V, L)$  and  $C_1(\delta, \Delta V, L)$  (multiplied by  $\Delta V^2$  and  $\Delta V^5$  respectively for visualization purposes) as a function of  $\delta$  for different values of  $\Delta V$  and  $L$  (top and bottom panel respectively). The obtained points correspond very well to the universal curves  $C_n(\delta, \Delta V) = A_n(\delta + 1)^2 \Delta V^{\nu_n}$ .

- [3] M. Glück, A. R. Kolovsky, and H. J. Korsh, *Phys. Rep.* **366**, 103 (2002).
- [4] E. E. Mendez and G. Bastard, *Physics Today* **46**, 34 (1993).
- [5] J. Bleuse, G. Bastard, and P. Voisin, *Phys. Rev. Lett.* **60**, 220 (1988).
- [6] J. Feldmann, K. Leo, J. Shah, D. A. B. Miller, J. E. Cunningham, T. Meier, G. von Plessen, A. Schulze, P. Thomas, and S. Schmitt-Rink, *Phys. Rev. B* **46**, 7252 (1992).
- [7] C. Waschke, H. G. Roskos, R. Schwedler, K. Leo, H. Kurz, and K. Köhler, *Phys. Rev. Lett.* **70**, 3319 (1993).
- [8] H. G. Roskos, C. Waschke, K. Victor, K. Kö, and H. Kurz, *Jpn. J. Appl. Phys.* **34**, 1370 (1995).
- [9] G. Lenz, I. Talanina, and C. M. de Sterke, *Phys. Rev. Lett.* **83**, 963 (1999).
- [10] R. Morandotti, U. Peschel, J. S. Aitchison, H. S. Eisenberg, and Y. Silberberg, *Phys. Rev. Lett.* **83**, 4756 (1999).
- [11] R. Sapienza, P. Costantino, D. Wiersma, M. Ghulinyan, C. J. Oton, and L. Pavesi, *Phys. Rev. Lett.* **91**, 263902 (2003).
- [12] H. Trompeter, W. Krolikowski, D. N. Neshev, A. S. Desyatnikov, A. A. Sukhorukov, Y. S. Kivshar, T. Pertsch, U. Peschel, and F. Lederer, *Phys. Rev. Lett.* **96**, 053903 (2006).
- [13] F. Dreisow, A. Szameit, M. Heinrich, T. Pertsch, S. Nolte, A. Tünnermann, and S. Longhi, *Phys. Rev. Lett.* **102**, 076802 (2009).
- [14] G. Corrielli, A. Crespi, G. D. Valle, S. Longhi, and R. Osellame, *Nat. Commun.* **4**, 2578 (2013).
- [15] H. Sanchis-Alepuz, Y. A. Kosevich, and J. Sánchez-Dehesa, *Phys. Rev. Lett.* **98**, 134301 (2007).
- [16] N. D. Lanzillotti-Kimura, A. Fainstein, B. Perrin, B. Jusserand, O. Mauguin, L. Largeau, and A. Lemaître, *Phys. Rev. Lett.* **104**, 197402 (2010).
- [17] M. B. Dahan, E. Peik, J. Reichel, Y. Castin, and C. Salomon, *Phys. Rev. Lett.* **76**, 4508 (1996).
- [18] S. R. Wilkinson, C. F. Bharucha, K. W. Madison, Q. Niu, and M. G. Raizen, *Phys. Rev. Lett.* **76**, 4512 (1996).
- [19] Z. A. Geiger, K. M. Fujiwara, K. Singh, R. Senaratne, S. V. Rajagopal, M. Lipatov, T. Shimasaki, R. Driben, V. V. Konotop, T. Meier, and D. M. Weld, *Phys. Rev. Lett.* **120**, 213201 (2018).
- [20] X.-Y. Guo, Z.-Y. Ge, H. Li, Z. Wang, Y.-R. Zhang, P. Song, Z. Xiang, X. Song, Y. Jin, L. Lu, K. Xu, D. Zheng, and H. Fan, *npj Quantum Inf.* **7**, 51 (2021).
- [21] R. Landauer, *IBM J. Res. Dev.* **1**, 223 (1957).
- [22] R. Landauer, *Philos. Mag.* **21**, 863 (1970).
- [23] M. Büttiker, *Phys. Rev. Lett.* **57**, 1761 (1986).
- [24] D. S. Fisher and P. A. Lee, *Phys. Rev. B* **23**, 6851 (1981).
- [25] A. D. Stone and A. Szafer, *IBM J. Res. Dev.* **32**, 384 (1988).
- [26] Y. Meir and N. S. Wingreen, *Phys. Rev. Lett.* **68**, 2512 (1992).
- [27] M. Wimmer, *Quantum transport in nanostructures: from computational concepts to spintronics in graphene and magnetic tunnel junctions*, Dissertationreihe der Fakultät für Physik der Universität Regensburg No. 5 (Univ.-Verl. Regensburg, 2009).
- [28] C. Caroli, R. Combescot, P. Nozieres, and D. Saint-James, *J. Phys C: Sol. St. Phys.* **4**, 916 (1971).
- [29] G. Stefanucci and C.-O. Almbladh, *Phys. Rev. B* **69**, 195318 (2004).
- [30] G. Stefanucci, *Phys. Rev. B* **75**, 195115 (2007).
- [31] E. Khosravi, G. Stefanucci, S. Kurth, and E. K. U. Gross, *Phys. Chem. Chem. Phys.* **11**, 4535 (2009).
- [32] A.-P. Jauho, N. S. Wingreen, and Y. Meir, *Phys. Rev. B* **50**, 5528 (1994).
- [33] M. Cini, *Phys. Rev. B* **22**, 5887 (1980).
- [34] G. Stefanucci and C.-O. Almbladh, *EPL* **67**, 14 (2004).
- [35] H. D. Cornean, C. Giansello, and V. Zagrebnov, *J. Phys. A: Math. Theor.* **43**, 474011 (2010).
- [36] R. Tuovinen, R. van Leeuwen, E. Perfetto, and G. Stefanucci, *J. Phys.: Conf. Series* **427**, 012014 (2013).
- [37] S. Latini, E. Perfetto, A.-M. Uimonen, R. van Leeuwen, and G. Stefanucci, *Phys. Rev. B* **89**, 075306 (2014).
- [38] R. Tuovinen, E. Perfetto, G. Stefanucci, and R. van Leeuwen, *Phys. Rev. B* **89**, 085131 (2014).
- [39] F. G. Eich, M. D. Ventra, and G. Vignale, *Phys. Rev. B* **93**, 134309 (2016).
- [40] P. P. Pal, S. Ramakrishna, and T. Seideman, *The Journal of Chemical Physics* **148**, 144707 (2018).
- [41] R. Tuovinen, E. Perfetto, R. van Leeuwen, G. Stefanucci, and M. A. Sentef, *New J. Phys.* **21**, 103038 (2019).
- [42] M. Ridley, M. Sentef, and R. Tuovinen, *Entropy* **21**, 737 (2019).
- [43] R. Taranko, T. Kwapiński, and T. Domański, *Phys. Rev. B* **99**, 165419 (2019).
- [44] J. P. Santos Pires, B. Amorim, and J. M. Viana Parente Lopes, *Phys. Rev. B* **101**, 104203 (2020).
- [45] M. Ridley, L. Kantorovich, R. van Leeuwen, and R. Tuovinen, *Phys. Rev. B* **103**, 115439 (2021).
- [46] M. Ridley, N. W. Talarico, D. Karlsson, N. L. Gullo, and R. Tuovinen, *J. Phys. A: Math. and Theor.* **55**, 273001 (2022).

- (2022).
- [47] Z. Cao, G. Zhang, H. Zhang, W.-X. He, C. Zeng, K. He, and D. E. Liu, *Phys. Rev. B* **106**, 075416 (2022).
- [48] N. Bushong, N. Sai, and M. Di Ventra, *Nano Lett.* **5**, 2569 (2005).
- [49] B. S. Popescu and A. Croy, *New J. Phys.* **18**, 093044 (2016).
- [50] T. Kloss, J. Weston, B. Gaury, B. Rossignol, C. Groth, and X. Waintal, *New J. Phys.* **23**, 023025 (2021).
- [51] B. S. Popescu and A. Croy, *Phys. Rev. B* **95**, 235433 (2017).
- [52] A. Suresh, R. D. Soares, P. Mondal, J. P. S. Pires, J. M. V. P. Lopes, A. Ferreira, A. E. Feiguin, P. Plecháč, and B. K. Nikolić, [arXiv:2210.06634](https://arxiv.org/abs/2210.06634).
- [53] C. W. Groth, M. Wimmer, A. R. Akhmerov, and X. Waintal, *New J. Phys.* **16**, 063065 (2014).
- [54] J. P. Santos Pires, N. A. Khan, J. M. Viana Parante Lopes, and J. M. B. Lopes dos Santos, *Phys. Rev. B* **99**, 205148 (2019).
- [55] G. H. Wannier, *Rev. Mod. Phys.* **34**, 645 (1962).
- [56] H. Fukuyama, R. A. Bari, and H. C. Fogedby, *Phys. Rev. B* **8**, 5579 (1973).
- [57] M. Holthaus and D. W. Hone, *Phil. Mag. B* **74**, 105 (1996).
- [58] A. Weiße, G. Wellein, A. Alvermann, and H. Fehske, *Rev. Mod. Phys.* **78**, 275 (2006).
- [59] H. Tal-Ezer and R. Kosloff, *The Journal of Chemical Physics* **81**, 3967 (1984).
- [60] S. Datta, *Electronic Transport in Mesoscopic Systems* (Cambridge University Press, 1995).
- [61] We define the left and right eigenvectors of  $\mathcal{H}_{\text{eff}}(\epsilon) = \mathbf{H}_C + \boldsymbol{\Sigma}^R(\epsilon) + \boldsymbol{\Sigma}^L(\epsilon)$  as  $\mathcal{H}_{\text{eff}}(\epsilon)|\Phi_n^R(\epsilon)\rangle = \lambda_n(\epsilon)|\Phi_n^R(\epsilon)\rangle$  and  $\langle\Phi_n^L(\epsilon)|\mathcal{H}_{\text{eff}}(\epsilon) = \langle\Phi_n^L(\epsilon)|\lambda_n(\epsilon)$ , with the eigenvalue written as  $\lambda_n(\epsilon) = \epsilon_n(\epsilon) - i\gamma_n(\epsilon)$ . We have that  $\langle\Phi_n^L(\epsilon)|$  form a dual basis to  $|\Phi_n^R(\epsilon)\rangle$ ,  $\langle\Phi_n^L(\epsilon)|\Phi_m^R(\epsilon)\rangle = \delta_{n,m}$ . However, since  $\mathcal{H}_{\text{eff}}(\epsilon)$  is non-hermitian, we have that  $|\Phi_n^R(\epsilon)\rangle \neq [|\Phi_n^L(\epsilon)\rangle]^\dagger$ . Notice that  $[|\Phi_n^L(\epsilon)\rangle]^\dagger \equiv |\Phi_n^L(\epsilon)\rangle$  are the right eigenstates of  $\mathcal{H}_{\text{eff}}^\dagger(\epsilon)$ .
- [62] In practice, to obtain the QPA to  $\mathbf{G}(\epsilon)$  we proceed as follows. (i) For each energy of the isolated central region,  $\epsilon_{C,n}$ , we start by computing the left/right eigenstates and eigenvalues of  $\mathcal{H}_{\text{eff}}(\epsilon_{C,n})$ . (ii) Then we select the eigenpair  $|\Phi_m^{R/L}(\epsilon_{C,n})\rangle$ ,  $\epsilon_m(\epsilon_{C,n}) - i\gamma_m(\epsilon_{C,n})$  with  $\epsilon_m(\epsilon_{C,n})$  closest to  $\epsilon_{C,n}$ . (iii) Sum over the contributions obtained in this way for each eigenenergy of the isolated central region  $\epsilon_{C,n}$ .
- [63] M. Abramowitz and I. A. Stegun, *Handbook of Mathematical Functions with Formulas, Graphs, and Mathematical Tables* (U.S. Government Printing Office, 1964).
- [64] T. Hartmann, F. Keck, H. J. Korsch, and S. Mossmann, *New J. Phys.* **6**, 2 (2004).